



PEARL

Metal pollutant pathways in cohesive coastal catchments: Influence of flocculation and biopolymers on partitioning and flux

Schindler, R. J.; Comber, S. D.W.; Manning, A. J.

Published in:

Science of the Total Environment

DOI:

[10.1016/j.scitotenv.2021.148800](https://doi.org/10.1016/j.scitotenv.2021.148800)

Publication date:

2021

Link:

[Link to publication in PEARL](#)

Citation for published version (APA):

Schindler, R. J., Comber, S. D. W., & Manning, A. J. (2021). Metal pollutant pathways in cohesive coastal catchments: Influence of flocculation and biopolymers on partitioning and flux. *Science of the Total Environment*, 795(0).
<https://doi.org/10.1016/j.scitotenv.2021.148800>

All content in PEARL is protected by copyright law. Author manuscripts are made available in accordance with publisher policies. Wherever possible please cite the published version using the details provided on the item record or document. In the absence of an open licence (e.g. Creative Commons), permissions for further reuse of content should be sought from the publisher or author.

2 **AVAILABLE AT:**

3 Science of The Total Environment 795:148800-148800 Article number 148800 Nov 2021

4 **Metal pollutant pathways in cohesive coastal catchments: Influence of**
5 **Flocculation and Biopolymers on Partitioning and Flux.**

6 **Authors:** Schindler, R.J.¹, Comber, S.D.W.^{1*} and Manning, A.J.^{2,3}

7 **Affiliations:**

8 1. School of Geography, Earth & Environmental Science, Plymouth University, UK.

9 2. School of Biological and Marine Sciences, Plymouth University, UK.

10 3. HR Wallingford Ltd, Howbery Park, Wallingford, UK.

11 *Corresponding author: sean.comber@plymouth.ac.uk

12 **ABSTRACT**

13 The impacts of the partitioning of potentially toxic metals (PTM) within the estuarine
14 environment is highly complex, but is of key significance owing to increases in populations
15 living within such sensitive environments. Although empirical data exist for the partitioning of
16 metals between the dissolved and particulate phases, little is known regarding the impacts of
17 extracellular polymeric substances (EPS) upon the flocculation of particles within such a
18 dynamic system nor the resultant influence on the distribution of metals between the particulate
19 and dissolved phases. This prevents regulators from fully understanding the fate and risks
20 associated with metals in estuaries. This study provides data associated with the simulation of
21 3 settlings typical of the turbulent mixing found in estuaries and partitioning of copper,
22 cadmium, nickel, arsenic, lead and zinc for 3 salinities (0, 15, 30 PSU) reflecting the full
23 salinity range from freshwater to seawater. Experiments were completed with and without the

24 presence of EPS, using kaolin as the mineral particulate. The results showed significant
25 differences between salinity, PTMs and turbulence for the experiments with and without EPS
26 present. Overall, salinity was the main factor controlling the PTM partitioning to sediment,
27 however the flocculation process did impact on the PTM distribution and with the addition of
28 EPS the impact was more pronounced. The data highlighted the importance of taking account
29 of EPS within any estuarine sediment process modelling, for relying on simple partitioning
30 with corrections for salinity would likely lead to significant bias.

31

32 **Keywords:** Potentially Toxic Metals; Partitioning; Flocculation; EPS; Salinity.

33

34 **1. INTRODUCTION**

35 The dispersion of potentially toxic metals (PTMs) into the aquatic environment poses a range
36 of environmental problems. PTMs are released from land-based sources: current and historical
37 mining and smelting industries, industrial and sewage effluents, landfill leachate as well as
38 common use of animal feeds, fertilizers and pesticides, surface runoffs and atmospheric
39 deposition (Taylor & Hudson-Edwards, 2008). They do not degrade, but can change form
40 (speciation) and/or move between the dissolved and particulate phases (partitioning). Global
41 concentrations of PTMs in coastal sediments have increased over 1985–2000 and can affect
42 the ecological balance of freshwater and marine environments for hundreds of years after
43 initial contamination.

44 Globally, large human populations are concentrated in the narrow zone adjacent to the coast.
45 Lowland rivers and estuaries provide a multitude of ecosystem services such as drinking
46 freshwater supply, fisheries, climate regulation, sheltered access to coastal water, coastal
47 protection, water purification and waste treatment (Millennium Ecosystem Assessment, 2005).
48 Estuaries also serve as nursery areas for many species, provide habitat to a high diversity of
49 sensitive organisms for the whole or part of their life cycle, and are characterized by a high
50 biological productivity. However, estuaries have also been used for the dilution and disposal
51 of waste worldwide (Spencer et al., 2006) which contributes to their deterioration. Bio-
52 assimilation and bio-accumulation of PTMs in aquatic organisms can reach pathogenic and
53 even lethal levels, endangering entire eco-systems and human health (Matta et al., 1999;
54 Hudson-Edwards et al., 1999). Danger to human health is particularly pronounced in the
55 developing world due to poor environmental regulation and a dependency on local water and
56 aquatic food (Luoma & Rainbow, 2008).

57

58 PTMs are transported as (1) **particulates** bound to sediments and 2) **solutes** in groundwater
59 and open channel flow. This distinction is an important consideration with respect to their
60 transportation, bioavailability and ultimate environmental fate (Comber et al., 1995). Reactions
61 in which PTMs are reversibly bound to the surface of the sediment matrix are referred to as
62 sorption processes. PTMs desorbed to the water column remain unconstrained and exhibit
63 much great mobility, bioavailability and hence toxicity. Measures to control or minimise
64 dispersion of particles will also control the environmental distribution of PTMs in their
65 particulate phase. In terms of grain-size, the highest metal concentrations are often found in the
66 finest-grained (such as silt- and clay-rich) sedimentary deposits because of the positive
67 relationship between grain surface area (and therefore increased adsorption sites) and metal
68 concentration or as a result of opposite electrical charge, in the case of cationic metals
69 (Zwolsman et al., 1993). Consequently, the particulate-borne phase dominates the transport of
70 PTMs (up to 90% of load, Miller et al., 2007) from land-based sources to the coastal zone
71 (Benoit et al., 1994) and leads to gradual dispersion and accumulation (Dennis *et al.*, 2003).

72 Prediction and management of PTMs transported from terrestrial sources to the ocean is
73 dependent on an accurate understanding of partitioning between soluble and particulate phases
74 at different spatial and temporal locations within a catchment. PTMs in bed and bank
75 sediments are not permanently fixed but can be periodically remobilized, desorbed, or
76 redistributed between the river to the sea via an estuary (Singh et al., 2005). The ambient
77 conditions that affect partitioning within fluvial and lacustrine environments (e.g., pH,
78 suspended particulate matter concentration (SPM), redox conditions, association with organic
79 carbon and colloidal material) become more complex across the river to sea gradient. Estuarine
80 waters are characterized by strong tidally-driven physicochemical gradients in e.g. salinity,
81 water density, flow velocity and turbulence regimes, and suspended matter composition (Elliott
82 and McLusky, 2002), which are important influences on the fate of metals. These factors lead

83 to the observed non-conservative behaviour for the majority of metal elements within estuaries
84 (Machado et al., 2016). Notably, estuaries experience saline intrusion resulting in chloro-
85 complexation and formation of insoluble salts with a counter-ion, most commonly sulphide
86 (Comber et al., 1996; Wells, 2019). Furthermore, contamination is expected to increase as more
87 sediments are mobilized with rising sea level and increasing storm frequency (DEFRA, 2014).

88 The sedimentary make up of most estuaries is dominated by fine-grained mud (silt and clay)
89 (Healey et al., 2002), which is key to the life cycle of indigenous sediment-dwelling organisms
90 (Black et al., 2002) and which influence the chemical nature of the substratum (Meadows et
91 al., 2012). What is less recognised with respect to the sorption, sedimentation and sediment
92 accumulation cycle is the role of flocculation. Flocculation is a dynamically active process
93 dependent on the electrostatic charging of the mineral, and which readily reacts to changes in
94 hydrodynamics, SPM concentration, salinity, organic content and mineralogy. Particles
95 aggregate through collisions to form ‘flocs’, comprising up to $\sim 10^6$ constituent particles
96 (Manning, 2004). Changes in turbulent shear stress (τ) may both promote floc aggregation and
97 disaggregation (Manning et al., 2017) and, together with salinity, can impose a maximum floc
98 size restriction on suspended sediments that vary spatially and temporally in response to tidal
99 cycles. As flocs grow in size their effective densities generally decrease (Klimpel & Hogg,
100 1986) and their settling velocities rise due to a Stokes’ Law relationship (Manning & Dyer,
101 1999). Typically, floc settling velocities are significantly quicker than for individual cohesive
102 particles ($\sim 1\text{-}5\ \mu\text{m}$ in diameter).

103 There is an increasing awareness that naturally occurring extracellular polymeric substances
104 (EPS), secreted by bacteria and microphytobenthos (principally diatoms) mediate sediment
105 dynamics in cohesive environments (Spears et al., 2007; Malarkey et al., 2015). EPS occurs at
106 mg/kg levels in sediments and like metals, will partition into the dissolved phase, where

107 Morelle et al., (2017) have reported soluble concentrations in the mg/l range driven by
108 phytoplankton excretion and microbenthos contributions; thus supporting their role in
109 influencing the flocculation dynamics (Hanlon et al., 2006).

110 Recent studies show that EPS binds particles together because molecules adhere to particle
111 surfaces, form elastic ‘bridges’ linking grains, fill void space and ultimately envelope grains
112 (Parsons et al., 2016). Once present, EPS is involved in cycles of sediment erosion, transport,
113 flocculation and deposition, exerting a significant influence on sediment dynamics (e.g.
114 Malarkey et al., 2015; Parsons et al., 2016). EPS therefore has the capacity to modulate
115 flocculation by influencing the binding potential of particles within each floc. Moreover, the
116 solubilisation and remineralization due to microbial activity could also affect the stability of
117 flocs (Kiørboe, 2001), via impacting floc size and settling velocity resulting in a more complex
118 sediment dynamics compared with pure-mineral dynamics (Lai et al., 2018).

119 The determination of particulate-borne PTM load is dependent on the accuracy of partitioning
120 coefficients for individual PTMs. However, significant gaps in our understanding exist in
121 cohesive estuarine environments where flocculation dictates SPM transport and deposition.
122 Knowledge of the association of PTMs with flocculated sediments is limited to a single study
123 in coastal waters (Koron et al., 2013). It is clear that the partitioning of PTMs between soluble
124 and particulate phases, and the flux of associated pollutants, are spatially and temporally
125 variable in response to changing floc characteristics within a tidal catchment. Further, the role
126 of EPS, ubiquitous in estuarine muds, in both the modulation of flocculation dynamics and
127 PTM partitioning is yet to be determined and so forms the focus of this study. It is hypothesized
128 that floc size and settling velocity of the SPM population directly influence key aspects of the
129 SPM-metal sorption:desorption processes via:

130 1) the residency time of remobilized sediments in the water column,

- 131 2) the surface area of SPM available for sorption exchange
- 132 3) the cycle of floc aggregation-disaggregation under changing salinity and turbulent
133 shear stresses over tidal times-scales promotes sorption-desorption exchanges
- 134 4) the ubiquitous presence of EPS may modulate floc characteristics, and consequently
135 sorption processes within an estuary
- 136 5) EPS may also directly influence partitioning by blocking sorption sites within the floc
137 matrix
- 138 6) EPS may impact on partitioning through complexation of metal ions with known
139 affinities for organic ligands such as copper and to a lesser extent zinc and nickel.

140 In addition, the amount of PTMs deposited in the particulate phase will change in response to
141 the mass settling flux (MSF) of sediments - the mass of sediment deposited over an area over
142 time – which is a function of spatial and temporal changes of the flocculated SPM population.
143 These experiments quantify, for the first time, the partitioning coefficients of PTMs in
144 flocculated SPM populations in estuaries. The study also comprises the first controlled
145 assessment of EPS modulation of flocculation dynamics and, by extension, PTM sorption
146 dynamics. By calculating MSF through unique floc measurement techniques, the settling flux
147 of particulate-borne PTMs (PSF) in cohesive estuaries is presented for the first time.

148 **2. MATERIALS & METHODS**

149 The experiments use an annular flume to physically model changing hydrodynamics, salinity
150 and EPS content at (i) **river**, (ii) **estuary** & (iii) **coastal** zones across an idealized mesotidal
151 muddy catchment to quantify:

- 152 1. The partitioning coefficients of common PTMs
- 153 2. The effects of EPS on partitioning coefficients of common PTMs
- 154 3. The effects of EPS on floc characteristics

155 4. The settling flux of particulate-borne PTMs (PSF)

156

157 **Table 1. Salinity and turbulent shear stress combinations of each experiment**
158 **(repeated with and without EPS addition).**

Salinity	Turbulent Shear Stress, τ
PSU	Pa
0	0.70 = τ_{Hi}
0	0.35 = τ_{Int}
0	0.10 = τ_{Low}
15	0.70 = τ_{Hi}
15	0.35 = τ_{Int}
15	0.10 = τ_{Low}
30	0.70 = τ_{Hi}
30	0.35 = τ_{Int}
30	0.10 = τ_{Low}

159

160 **2.1 Annular Flume & Turbulent Shear Stress**

161 This study utilised a mini-annular flume to create a consistent and repeatable turbulent
162 environment. The annular flume has an outer diameter of 1.2 m, a channel width of 0.1 m and
163 a maximum depth of 0.15 m, with a motor-driven rotating roof to create the flow for cohesive
164 sediment experiments (Manning & Dyer, 1999). Maximum flow speeds of approximately 0.7
165 m s⁻¹ can be produced in the lower half of the water column, created by 10 mm deep paddles

166 attached to the underside of the roof. Three turbulent shear stresses, τ , were used to represent
167 variations in hydrodynamic forcing within an estuary (Manning et al., 2009) (Table 1). Each
168 experiment was undertaken twice: Once with a purely mineral suspended particulate matter
169 (*abiotic* case), and repeated with the addition of EPS (*biotic* case).

170 **2.2 PTM Additions**

171 Six potentially toxic metals (PTMs) typical of mining wastes associated with sulphidic ores
172 found in mineral rich locations across the globe were used in each experimental run: arsenic
173 (As), cadmium (Cd), copper (Cu), nickel (Ni), lead (Pb) and zinc (Zn). They are amongst the
174 PTMs considered as Priority Substances, Priority Hazardous Substances and Specific
175 Pollutants by the EU's Water Framework Directive (DEFRA, 2014) and routinely assessed for
176 the UK's Marine Management Organisation marine licence applications.

177 Spiking concentrations were based on the expected partitioning behaviour of the elements to
178 ensure dissolved concentrations would be measurable after partitioning and dilution. Literature
179 suggests partitioning to the sediment will increase in the order Ni<Cd<As<Zn<Cu<Pb based
180 on physio-chemical characteristics of the elements themselves as well as their interactions with
181 saline matrices (Comber et al., 1996). Consequently, higher concentrations of lead were spiked
182 into solution compared with nickel as it was expected that lead would partition strongly to the
183 particulates leaving little in the dissolved phase to analyse; whereas nickel would be expected
184 to remain predominantly in solution. The concentration of metal spiked into the flume reflected
185 the partitioning with concentration additions ranging from 0.1 mg L⁻¹ for Ni to 2 mg L⁻¹ for
186 lead. The concentration of each PTM in each water sample was determined through ICP-MS
187 post-experiments. For saline runs, samples were diluted by a factor of 5 in order to avoid salt
188 matrix interference in the ICP-MS analysis.

189 **2.3 Suspended Particulate Matter**

190 *Mineral (Abiotic) Experiments*

191 The sediment component comprised kaolin clay with a median grain size of 6 μm . The depth-
192 averaged suspended particle matter concentration (SPMC) was maintained at 1.0 g L^{-1} for all
193 abiotic experiments. Sediment slurries were prepared using 38.0 g of kaolin in 0.5 L of ultra-
194 pure water.

195 *Biotic Experiments*

196 Xanthan gum, a versatile fine-powdered polysaccharide produced from *Xanthomonas*
197 *campestris* bacterium, is used as a proxy for EPS. It becomes soluble when added to water and
198 has been previously been used as a proxy for biological cohesion in studies on biomediated
199 sediment transport (e.g., Malarkey et al, 2015; Parsons et al., 2016). EPS concentrations on
200 surface sediments may be up to 5% (dry weight) in intertidal muds (Taylor & Patterson, 1998)
201 and >1% in freshwater muds (Gerbersdorf et al., 2009). Lower concentrations of EPS (0.01–
202 0.1%) have been found pervasively distributed in sandy muds and sands with low mud content
203 (e.g. Patterson et al., 2000). EPS content of the SPM in these experiments was held at 2% - an
204 intermediate value spanning surface deposits (most liable to become suspended) in freshwater
205 and estuarine locations. Kaolin (37.24 g) and EPS (0.76 g) were mixed when dry to ensure
206 homogeneity before the addition of 0.5 L of ultra-pure water to form a slurry.

207 Gravimetric analysis of extracted water samples were used to ensure the ambient SPMC was
208 within required experimental tolerances across all experiments.

209 **2.4 Experimental Procedure**

210 The capacity of the flume is 38 L and it was filled with 37.5 L of ultra-pure water before the
211 start of each experiment. For saline experiments, salt was progressively added and the flume
212 circulated to mix the salt until the required salinity was reached. The following procedure was
213 followed:

- 214 1) Metal standards were directly introduced into the water, and mixed through flume
215 circulation for 5 minutes.
- 216 2) Trial experiments revealed that the pH of the water after the introduction of metal standards
217 was ~4.5, significantly lower than found in estuaries. A buffer was added to the water to
218 ensure that $\text{pH} = 8.2 \pm 0.1$.
- 219 3) 3 x 15 ml water samples were taken for Inductively Coupled Plasma-Mass Spectrometry
220 (ICP-MS) analysis to determine the precise initial PTM dissolved concentrations. Samples
221 were diluted 5 fold with ultra-pure water in order to reduce the salt matrix (for 15 and 30
222 PSU)
- 223 4) The sediment slurry (0.5 L) was introduced into the flume and mixed at τ_{Hi} for 1 minute,
224 and a second set of water samples taken for ICP analysis.
- 225 5) The mixed sediment slurries were sheared in the flume for 30 minutes at τ_{Hi} . This duration
226 of shearing was pre-determined in accordance with theoretical flocculation time (van
227 Leussen, 2004).
- 228 6) To obtain floc and water samples, the rotation was stopped for approximately 6-8 seconds,
229 although flow in the flume still continued through inertia, maintaining particles in
230 suspension throughout this period (Manning & Whitehouse, 2009). 50 ml samples were
231 extracted using a glass pipette at mid-height of the flow: (1) A sample for floc
232 characterisation, (2) three samples for ICP analysis, and (3) a sample for gravimetric
233 quantification of the SPMC.
- 234 7) Steps 5& 6 were repeated at τ_{Int} and τ_{Low}
- 235 The flume was subsequently emptied and cleaned using a high-pressure sprayer and detergents
236 in preparation for the next experiment.

237 **2.5 PTM Concentrations of Water Samples**

238 For each experiment, the mean soluble PTM concentrations from initial, sediment-free
239 conditions (see Step 4) were established based on three replicate water samples. Dissolved
240 PTM concentrations were measured. Particulate PTM concentrations were calculated assuming
241 any loss from the dissolved phase was a result of sorption to the particulate matter. A control
242 experiment showed insignificant sorption to the flume apparatus nor loss whilst filtering (2%
243 hydrochloric acid cleaned) 0.4 μm Sartorius cellulose acetate membranes. Subsequently each
244 experiment yielded three mean values concentration in the dissolved phase, C_d , for each
245 turbulent condition (Step 7): $a = \tau_{Hi}$, $b = \tau_{Int}$ and $c = \tau_{Low}$. The data was used to determine
246 partitioning coefficients, K_p , which give information on the integrated effects of adsorption and
247 desorption processes:

$$248 \quad K_p = \frac{C_s}{C_d} \quad [\text{Eq. 1}]$$

249 where C_d is the concentration in the dissolved phase (mg ml^{-1}) and C_s is the concentration of
250 metal in the particulate phase (initial PTM concentration – C_d , mg g^{-1}).

251 **2.6 Floc Characterisation**

252 Floc sample populations were characterized using LabSFLOC (*Laboratory Spectral*
253 *Flocculation Characteristics*), a video-based instrument developed at Plymouth University.
254 SPM samples were taken from the water column using a pipette and transferred to the
255 LabSFLOC settling column following protocols outlined in Manning et al., 2017. The SPM
256 was recorded by the video camera as it was settling. The observed flocs were measured within
257 a reference volume of water (0.4 L). Floc size (equivalent spherical diameter, D) and settling
258 velocity (W_s) were determined for each individual floc directly from video recordings. The
259 effective density (ρ_{eff}) of each floc was calculated by applying Stokes' Law relationship,
260 (Manning et al., 2017):

261
$$\rho_{eff} = (\rho_f - \rho_w) = \frac{W_s 18 \mu}{D^2 g} \quad [\text{Eq. 2}]$$

262 where ρ_{eff} is the difference between the floc bulk density (ρ_f) and the water density (ρ_w) and μ
263 is kinematic viscosity. Mass settling flux, MSF , is defined as the product of the settling velocity
264 and SPM concentration (Manning, 2004).

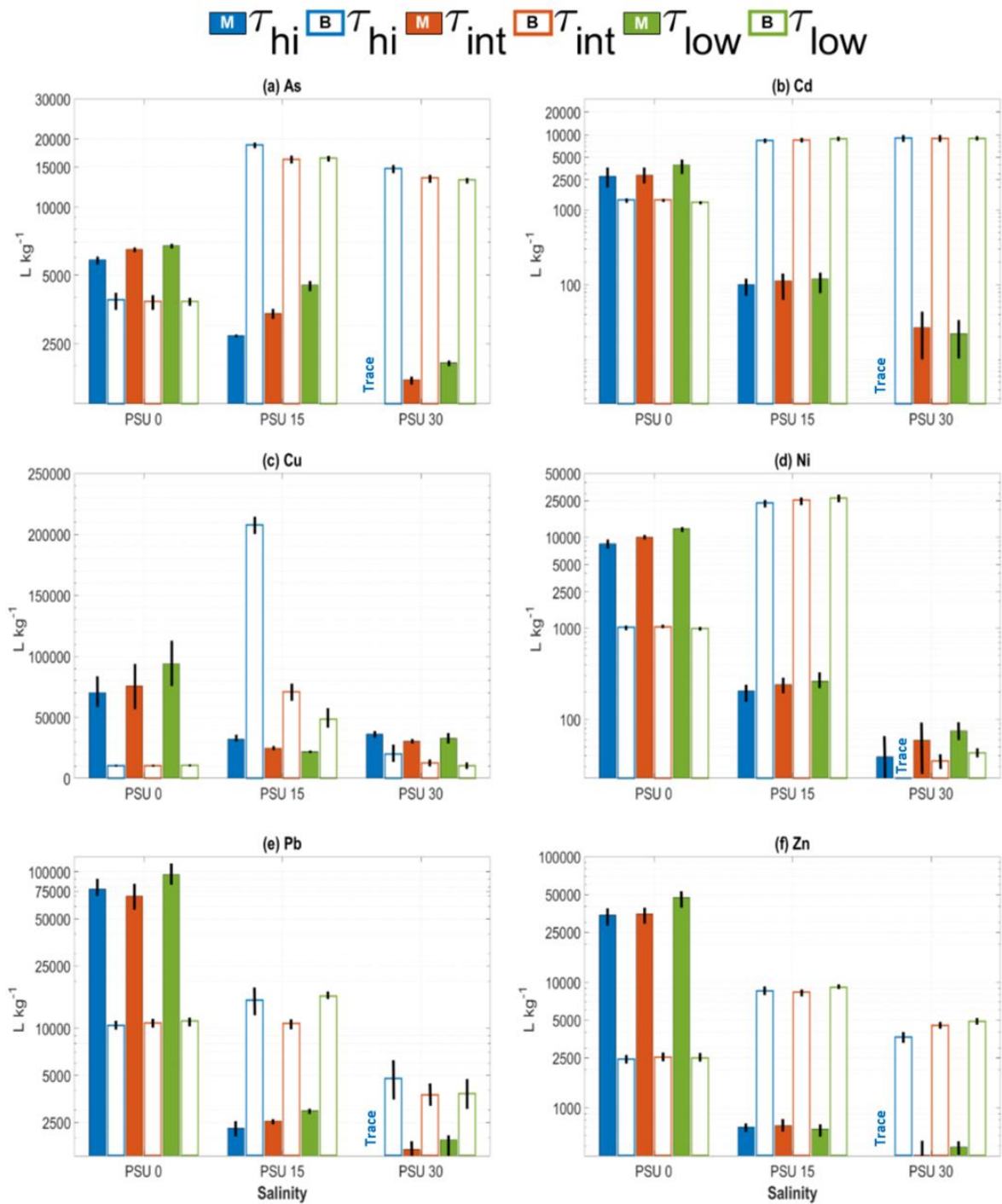
265 **3. RESULTS AND DISCUSSION**

266 **3.1 PTM Sorption and Partitioning**

267 Mean K_p values with 95% confidence intervals for each PTM in each experiment are shown in
268 Figure 1 & Tables S1 and S2 of the Electronic Supporting Information. $K_{p(\text{Min})}$ refers to mineral
269 SPM experiments; $K_{p(\text{Bio})}$ refers to biotic SPM experiments. Large $K_{p(\text{Min})}$ and $K_{p(\text{Bio})}$ values
270 under initial τ_{Hi} conditions indicate that the majority of physio-chemical processes resulting in
271 adsorption to the floc field occur rapidly (seconds to minutes) (Comber et al., 1996).

272 There are clear trends in the partitioning of the metals across the varying salinities. For the
273 mineral only phase partition coefficients ($K_{p(\text{Min})}$) clearly decrease with rising salinity across all
274 turbulence shear stresses for As, Cd, Ni, Pb and Zn, with a less distinct trend for Cu (Figure 1
275 and Table S2). The magnitudes of the partition coefficients are of the same order as reported
276 in the literature and the observed trends driven by a combination of chloro-complexation,
277 electrostatic competition and mass effects (Comber et al., 1995, Heiro et al., 2014; van der
278 Auweraert, 2018). Overall $K_{p(\text{Min})}$ partition coefficients followed the order
279 $\text{Pb} > \text{Cu} > \text{Zn} > \text{Ni} > \text{As} > \text{Cd}$ from highest to lowest.

280 The impact of organic chemicals on the partitioning of metals between water and sediment has
281 been explored previously, but mostly by looking at empirical relationships (DeFonseca et al.,
282 2013; Nho et al., 2018).



283

284 **Figure 1. Partitioning coefficients, K_p , for each PTM for each experimental run. Solid**
 285 **bars indicate results for mineral SPM; bars with colour outlines indicate**
 286 **results for biotic SPM. Note that all y-axes are logarithmic with the exception**
 287 **of (c) which is linear. Error bars are confidence intervals at 95%.**

288 However, the partitioning behaviour after the addition of the EPS was considerably different.
289 The magnitude of $K_{p(\text{Bio})}$ in freshwater (PSU 0, clear bars) show no statistical difference across
290 turbulence regimes for any of the PTMs, but were lower than the equivalent coefficients for
291 the mineral only $K_{p(\text{min})}$, for each PTM (reductions in K_p resulting from the addition of EPS in
292 freshwater are, from largest to smallest: Zn>Ni>Cu=Pb>Cd>As; Table 2). This indicates that
293 sorption processes occur in the initial τ_{Hi} conditions, with minimal physio-chemical changes
294 resulting from subsequent reductions in turbulent shear stress. All $K_{p(\text{Bio})}$ values were lower
295 than $K_{p(\text{Min})}$ equivalents (Table S1).

296 For the saline samples $K_{p(\text{Bio})}$ was, with the exception of lead and nickel, higher than the
297 freshwater samples. For all PTMs other than Cd, $K_{p(\text{Bio})}$ was lower in the PSU30 samples across
298 all turbulence than the PSU15 case, again largely reflecting the trend of the $K_{p(\text{Min})}$ dataset.
299 However, other than for Cu and Ni at PSU30, in all cases $K_{p(\text{Bio})}$ was greater than the equivalent
300 $K_{p(\text{Min})}$. Changes in shear stress turbulence impacted on the partitioning of the metals to varying
301 degrees, but generally differences were more subtle than observed with changing the salinity.

302 For freshwater As, Cu, Ni, Pb and Zn exhibit marginal, but not statistically different increases
303 in $K_{p(\text{Min})}$ across τ_{Hi} – τ_{Low} . $K_{p(\text{Bio})}$ values for freshwater were effectively identical. At higher
304 salinities, other than for copper at PSU15 where $K_{p(\text{Bio})}$ decreased across τ_{Hi} – τ_{Low} all other
305 PTMs remained consistent (Table S3). For $K_{p(\text{Min})}$ across τ_{Hi} – τ_{Low} significant increases for both
306 PSU15 and PSU30 were observed for As and to a degree Pb and Ni, with no statistical
307 differences for the other PTMs.

308

309 **Table 2. $K_p(\text{Bio}):K_p(\text{Min})$ ratio for each PTM for each turbulence regime and salinity.**

As	τ_{Hi}	τ_{Int}	τ_{Low}	Mean
PSU 0	0.66	0.59	0.57	0.61
PSU 15	6.91	4.78	3.62	5.10
PSU 30	10.9	7.77	6.41	8.36

310

Cd	τ_{Hi}	τ_{Int}	τ_{Low}	Mean
PSU 0	0.48	0.46	0.32	0.42
PSU 15	83.7	75.7	73.8	77.8
PSU 30	3507	331	401	1413

311

Cu	τ_{Hi}	τ_{Int}	τ_{Low}	Mean
PSU 0	0.14	0.14	0.11	0.13
PSU 15	6.50	2.87	2.20	3.86
PSU 30	0.55	0.42	0.28	0.42

312

Ni	τ_{Hi}	τ_{Int}	τ_{Low}	Mean
PSU 0	0.12	0.10	0.08	0.10
PSU 15	116	106	102	108
PSU 30	0.58	0.59	0.57	0.58

313

Pb	τ_{Hi}	τ_{Int}	τ_{Low}	Mean
PSU 0	0.13	0.15	0.12	0.13
PSU 15	6.58	4.19	5.39	5.39

PSU 30	3.14	2.24	1.97	2.45
---------------	------	------	------	------

314

Zn	τ_{Hi}	τ_{Int}	τ_{Low}	Mean
PSU 0	0.07	0.07	0.05	0.07
PSU 15	12.1	11.6	13.4	12.4
PSU 30	8.83	10.8	10.0	9.88

315 The dataset showed that there are considerable differences in adsorption for all PTMs based on
316 a combination of chemistry (predominantly chloro-complexation) but also contributions from
317 the interaction between the EPS, inorganic particles and EPS-metal complexation
318 characteristics. Previous studies have shown the influence of particulate organic matter, of
319 which EPS would be significant component, to be a controlling factor in the partitioning of
320 metals in estuaries, but itself will be influenced by salinity (Turner et al., 2004). Furthermore,
321 colloidal material in estuaries which comprises a mostly poorly defined proportion of organic
322 and inorganic species also influence the partitioning of PTMs (Wang and Wang, 2016). The
323 complex interplay between these factors ultimately determines the partitioning characteristics
324 of the PTMs (Feng et al., 2017).

325 Under freshwater conditions $K_{p(Min)} > K_{p(Bio)}$ for all PTMs. Conversely, at 15 PSU, $K_{p(Bio)} >$
326 $K_{p(Min)}$ for all PTMs resulting from both a reduction in adsorption for mineral SPM and
327 increases for biotic SPM when compared with freshwater. For most PTMs the reduction in
328 turbulent shear stress causes adsorption in both mineral and biotic SPM to change in the same
329 manner, reflecting physical, rather than chemical control mechanisms. However, for As and Pb
330 $K_{p(Min)}$ values increase while (much larger) $K_{p(Bio)}$ values decrease.

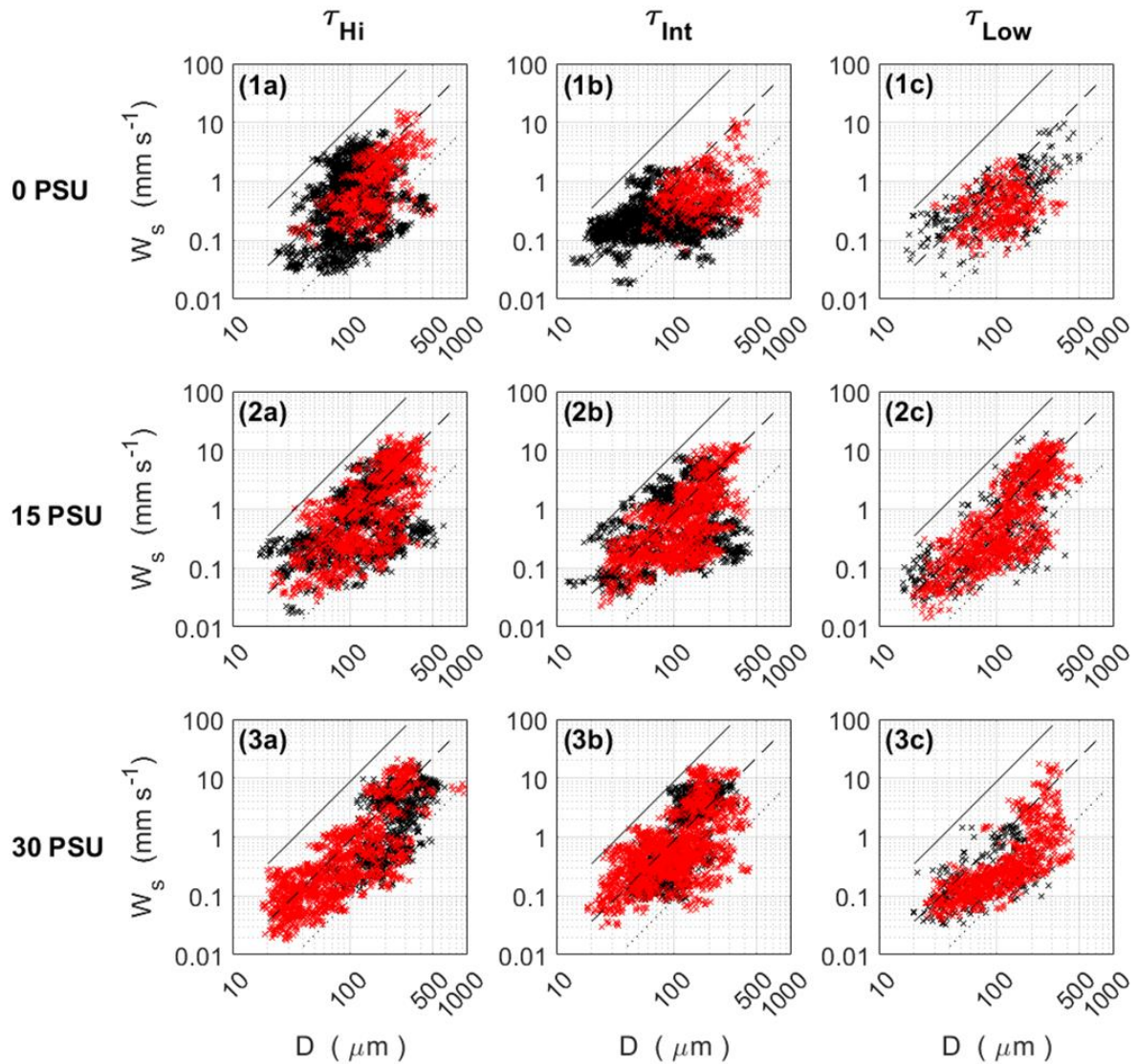
331 **3.2 Flocculation Characteristics**

332 Figure 2 shows the distribution of size versus settling velocity of flocculated particles within
333 the SPM for each experimental scenario. Figure 3 and Table S4 summarise the mean primary

334 characteristics of each floc population. Mean floc size for mineral SPM ($D_{(Min)}$), under τ_{Hi}
335 increases with salinity, reflecting the improved efficiency of flocculation under increasing
336 electrostatic charging of the sediment. Mean settling velocity ($W_{s(Min)}$), rises 3-fold under high
337 shear stresses, with commensurate reductions in mean effective density (ρ_{eff}), following Stokes'
338 Law (Eq. 2) (Manning and Dyer, 1999). The reduced density of the floc population reflects the
339 small increase in mean porosity ($Por_{(Min)}$). The total surface area (A_{min}) of a floc population is
340 a function of the floc size, frequency (n), and SPM concentration ($SPMC$) and is shown to
341 increase with salinity under τ_{Hi} conditions (Figure 3). $SPMC_{(Min)}$, however, decreases as a
342 result of higher settling velocities of larger, less dense flocs (Klimpel and Hogg, 1986).
343 Similarly, the floc frequency ($n_{(Min)}$) declines, which is both a function of lower $SPMC_{(Min)}$ and
344 more efficient flocculation, which results in larger flocs comprised of more primary particles
345 (Manning, 2004). This indicates that surface area is principally controlled by floc size (D)
346 rather than floc frequency (n) and $SPMC$. The mass settling flux (MSF) is a function of settling
347 velocity (W_s), effective floc density (ρ_{eff}) and $SPMC$. $MSF_{(Min)}$ under τ_{Hi} conditions increases
348 significantly from 1.9 to 5.3 g m⁻² s⁻¹ from 0 – 30 PSU, a factor of 2.5, indicating that increases
349 in settling velocity ($W_{s(Min)}$) dominate over reductions in effective density (ρ_{eff}) and total
350 particulate matter concentrations ($SPMC$).

351 Under τ_{Int} conditions, $D_{(Min)}$ rises from 0 – 15 PSU then falls from 15 – 30 PSU, in contrast to
352 the constant increase seen for τ_{Hi} . $D_{(Min)}$ is also lower than under τ_{Hi} conditions for each salinity,
353 notably for 30 PSU where $D_{(Min)}$ is half that of τ_{Hi} conditions. $W_{s(Min)}$ increases with salinity but
354 is also lower than τ_{Hi} conditions. Conversely, $\rho_{eff(Min)}$ is statistically similar for 0 PSU and higher
355 for saline conditions than τ_{Hi} , exhibiting a rise and fall around 15 PSU commensurate with
356 changes in $D_{(Min)}$. These contrasts with τ_{Hi} reflect the lower rate of collision under a reduced
357 turbulent shear stress.

358



360

361

362 **Figure 2: Relationship between flocculation size, D , and settling velocity, W_s , for all experiments.**

363 **Both axes are logarithmic. Each observation represents a single flocculation within the**

364 **SPM population. Black observations are for mineral SPM; red observations**

365 **are for biotic SPM. Diagonal lines show different values of effective density,**

366 **ρ_{eff} , for reference: 1600 (—), 160 (- - -) and 16 (.....) kg m^{-3}**

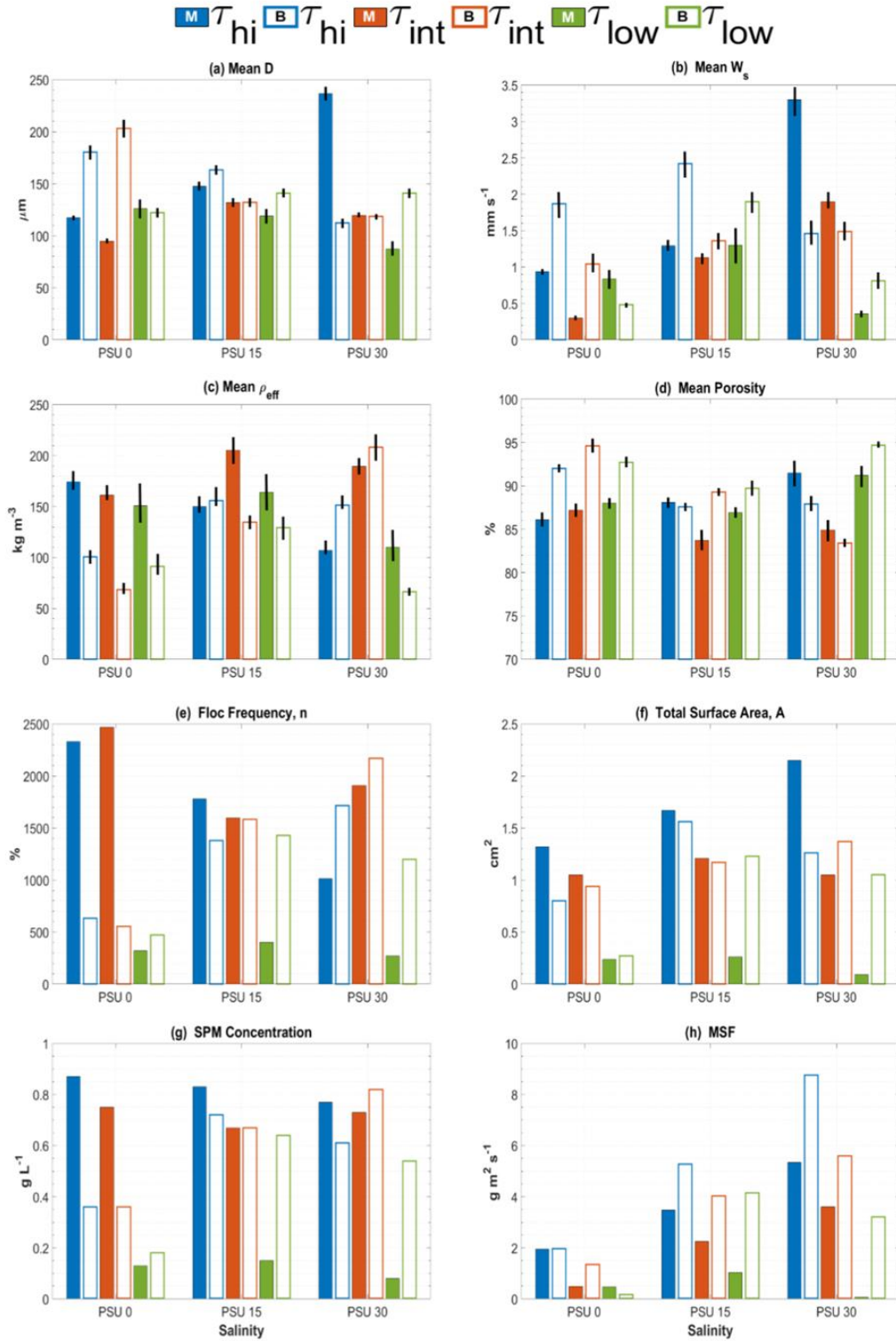
367

368

369 $A_{(Min)}$ shows a similar rise and fall around 15 PSU, despite an inverse pattern in $n_{(Min)}$ and
370 $SPMC_{(Min)}$. Compared with τ_{Hi} conditions, $A_{(Min)}$ is lower for τ_{Int} to a very similar degree seen
371 for $D_{(Min)}$, indicating that $D_{(Min)}$ principally controls surface area (Figure 2). $SPMC_{(Min)}$ is also
372 consistently lower in τ_{Int} , despite slower mean settling velocities, which is indicative of the
373 reduced turbulent energy available to maintain particles in suspension. $MSF_{(Min)}$ is reduced as
374 a consequence of both lower $SPMC_{(Min)}$ and $W_{s(Min)}$, despite higher mean effective density at
375 15 and 30 PSU.

376 Under τ_{Low} conditions, the mean floc size ($D_{(Min)}$) is the largest for mineral SPM under
377 freshwater conditions. Conversely, under saline conditions $D_{(Min)}$ values are smaller than other
378 turbulence regimes. $D_{(Min)}$ at 15 PSU is statistically similar but decreases 30 PSU. The mean
379 settling velocity ($W_{(min)}$) rises between 0 PSU and 15 PSU and is higher than the equivalent
380 under intermediate shear stress conditions, but falls at 30 PSU then falls significantly at 30
381 PSU. Floc frequency, $n_{(Min)}$, and $SPMC_{(min)}$ are considerably lower at each salinity than for
382 other turbulence regimes. This indicates that turbulent shear stress is insufficient to suspended
383 most of the SPM at the measurement height in the water column, despite $W_{s(Min)}$ values
384 comparable with higher turbulence regimes. Consequently, $A_{(Min)}$ is significantly lower under
385 τ_{Hi} and τ_{Int} conditions. $MSF_{(Min)}$ under 0 PSU is $0.46 \text{ g m}^{-2} \text{ s}^{-1}$, rising to 1.0 (15 PSU) and then
386 dropping to 0.08 (30 PSU), reflecting the response of both $W_{s(Min)}$ and $SPMC_{(Min)}$ to changes in
387 salinity.

388 The EPS floc data show some interesting differences in behaviour to the equivalent mineral
389 tests. Contrary to that observed for mineral SPM, floc size ($D_{(Bio)}$) clearly decreases in a step-
390 wise manner under τ_{Hi} conditions as salinity increases (Figure 3), where as the mean settling
391 velocity ($W_{s(Bio)}$) increases as salinity increases from 0 – 15 PSU, but then decreases at 30 PSU.



392

393 **Figure 3: Primary floc characteristics for the varying salinity and turbulence. Error bars**
 394 **in (a) – (d) are confidence intervals at 95%. Solid bars indicate results for mineral SPM;**
 395 **bars with colour outlines indicate results for biotic SPM.**

396 Changes in floc density ($\rho_{eff(Bio)}$) are commensurate with those for $W_{s(Bio)}$ driven by changes in
397 porosity ($Por_{(Bio)}$) which shows an inverse relationship to $W_{s(Bio)}$ and $\rho_{eff(Bio)}$. $SPMC_{(Bio)}$
398 increases from 0 to 15 PSU, then drops again at 30 PSU, reflecting changes in the mean density
399 of the flocs, which dominates over the decrease in floc size ($D_{(Bio)}$) and increase in floc
400 frequency ($n_{(Bio)}$). $MSF_{(Bio)}$ under τ_{Hi} conditions increases significantly with salinity by a factor
401 of 4.5. It is clear that the higher MSF for the biotic SPM is driven by a lower settling velocity
402 and higher effective density compared with mineral-only flocs (Figure 3).

403 Under τ_{Int} conditions, $D_{(Bio)}$ decreases with salinity as seen for the high turbulence tests (Figure
404 3). This is contrary to the rise and fall of $D_{(Min)}$ under τ_{Int} . Notably, $D_{(Bio)}$ is the largest mean
405 floc size across all of the EPS experiments. Mean settling velocities ($W_{s(Bio)}$) rise from 0 to 30
406 PSU, with values around half those seen for τ_{Hi} , as does the floc density ($\rho_{eff(Bio)}$) (Figure 3).
407 Compared with $W_{s(Min)}$ under τ_{Int} conditions, $W_{s(Bio)}$ is higher for 0 and 15 PSU, but lower at 30
408 PSU, which is the opposite to the behaviour of the floc density. At the intermediate turbulence,
409 the total surface area of the floc ($A_{(Bio)}$) increased steadily with salinity consistent with the floc
410 frequency and $SPMC_{(Bio)}$. Given the reduction in $D_{(Bio)}$ it can be concluded that initially the
411 SPM is comprised of large flocs which disaggregate into smaller flocs as salinity increases,
412 yielding an increase in total surface area. $SPMC_{(Bio)}$ is maintained at a relatively high
413 concentration because of floc density differences ($\rho_{eff(Bio)} < \rho_{eff(Min)}$). $MSF_{(Bio)}$ values increase
414 with salinity under intermediate shear conditions in a similar manner seen for τ_{Hi} , resulting
415 from increases in $W_{s(Bio)}$ and $SPMC_{(Bio)}$ which negate reductions in $\rho_{eff(Bio)}$ (Figure 3). However,
416 τ_{Int} values are significantly lower than τ_{Hi} for all salinities. Conversely, biotic SPM yields higher
417 $MSF_{(Bio)}$ values than $MSF_{(Min)}$ under τ_{Int} from freshwater to full salinity.

418 Under the lowest turbulence conditions the floc size ($D_{(Bio)}$) only exhibits a small increase with
419 salinity compared with a reduction in size for $D_{(Min)}$. Mean settling velocity ($W_{s(Bio)}$) and floc
420 density ($\rho_{eff(Min)}$) both rise between 0 and 15 PSU, but then decrease at 30 PSU. Floc frequency

421 (n), surface area $A_{(Bio)}$ and $SPMC_{(Bio)}$ all show the same trend of an increase from 0 to 15 PSU
422 then a slight decrease at 30 PSU (as was the case for the mineral tests) but in all cases the
423 overall magnitudes of the values were significantly higher in the case of the EPS tests.
424 However, the mass settling flux ($MSF_{(bio)}$) at 0 PSU was significantly lower than the equivalent
425 mineral value, but under saline conditions $MSF_{(Bio)}$ was greater for the low turbulence tests.

426 Overall, for mineral SPM, an increase in salinity promotes floc growth at τ_{Hi} , reflecting the
427 electrostatic charging of the sediment. $D_{(Min)}$ is positively related to salinity and doubles from
428 freshwater to seawater salinity. The full seawater flocs under τ_{Hi} exhibit settling velocities
429 ($W_{s(Min)}$) and effective floc density ($\rho_{eff(Min)}$) more than 3-times slower and were nearly twice as
430 dense. Conversely, there is a reduction in $D_{(Bio)}$ and a commensurate increase in n under τ_{Hi} and
431 τ_{Int} conditions as salinity increases. This indicates that salinity acts to reduce the influence of
432 EPS in binding particles. Notably, the largest mean floc size across all experiments is for biotic
433 SPM in freshwater. This indicates that flocculation efficiency is enhanced by the presence of
434 EPS in freshwater (Zhoa et al., 2011), generating larger, more porous flocs with lower densities
435 (Klimpel and Hogg, 1999). However, in saline conditions differences in porosity between
436 mineral and biotic SPM varies and is dependent on the shear stress (τ). This is obviously a key
437 variable within the estuarine environment where owing to tidal fluctuations (ebb and flow, neap
438 and spring), varying river water flows and estuarine topography and bathymetry the shear stress
439 is highly variable throughout its length (Manning, 2004).

440 $D_{(Min)}$ drops with τ for saline conditions. This is because collisions facilitating floc formation
441 from primary particles are less numerous in lower turbulence. Conversely, mean floc size and
442 frequency and $SPMC$ are notably higher for biotic SPM under τ_{Low} saline conditions, despite
443 higher settling velocities, indicative of the capacity of EPS to maintain flocs as turbulent mixing
444 decreases. Total surface area is an important consideration with respect to the availability of
445 sorption sites of the suspended sediment. It is a function of floc size and frequency. The total

446 surface area of mineral SPM is principally controlled by changes in floc size for τ_{Hi} and τ_{Int}
447 conditions, but under τ_{Low} conditions $n_{(Min)}$ dictates $A_{(Min)}$. $A_{(Bio)}$ is principally a function in $n_{(Bio)}$
448 with the exception of τ_{Hi} conditions across 15-30 PSU.

449 Mass settling flux increases with salinity for both mineral and biotic SPM, and both exhibit a
450 stepwise reduction across turbulent regimes for each salinity. Under saline conditions $MSF_{(Bio)}$
451 is substantially higher than $MSF_{(Min)}$, most notably under the lowest turbulent shear stress due
452 to the high residency time of flocs containing EPS. Typically, larger flocs have faster settling
453 velocities, but have a lower density and are therefore more porous. Consequently although the
454 SPM concentration and density are lower, mass settling fluxes can increase because the settling
455 rate outweighs the reductions in SPMC. Overall it can be evidenced in this study that the
456 presence of EPS leads to more complex sediment dynamics compared with a pure mineral
457 system (Lai et al., 2018).

458 3.3 *Settling Flux of Particulate PTMs*

459 The data from this study allows, for the first time, the sediment flocculation characteristics to
460 be combined with the observed sorption characteristics to explore the impacts of the
461 flocculation process on the partitioning of the PTMs. Consequently, it is possible to derive the
462 settling flux of the particulate PTM fraction for each PTM under each experimental scenario:

463

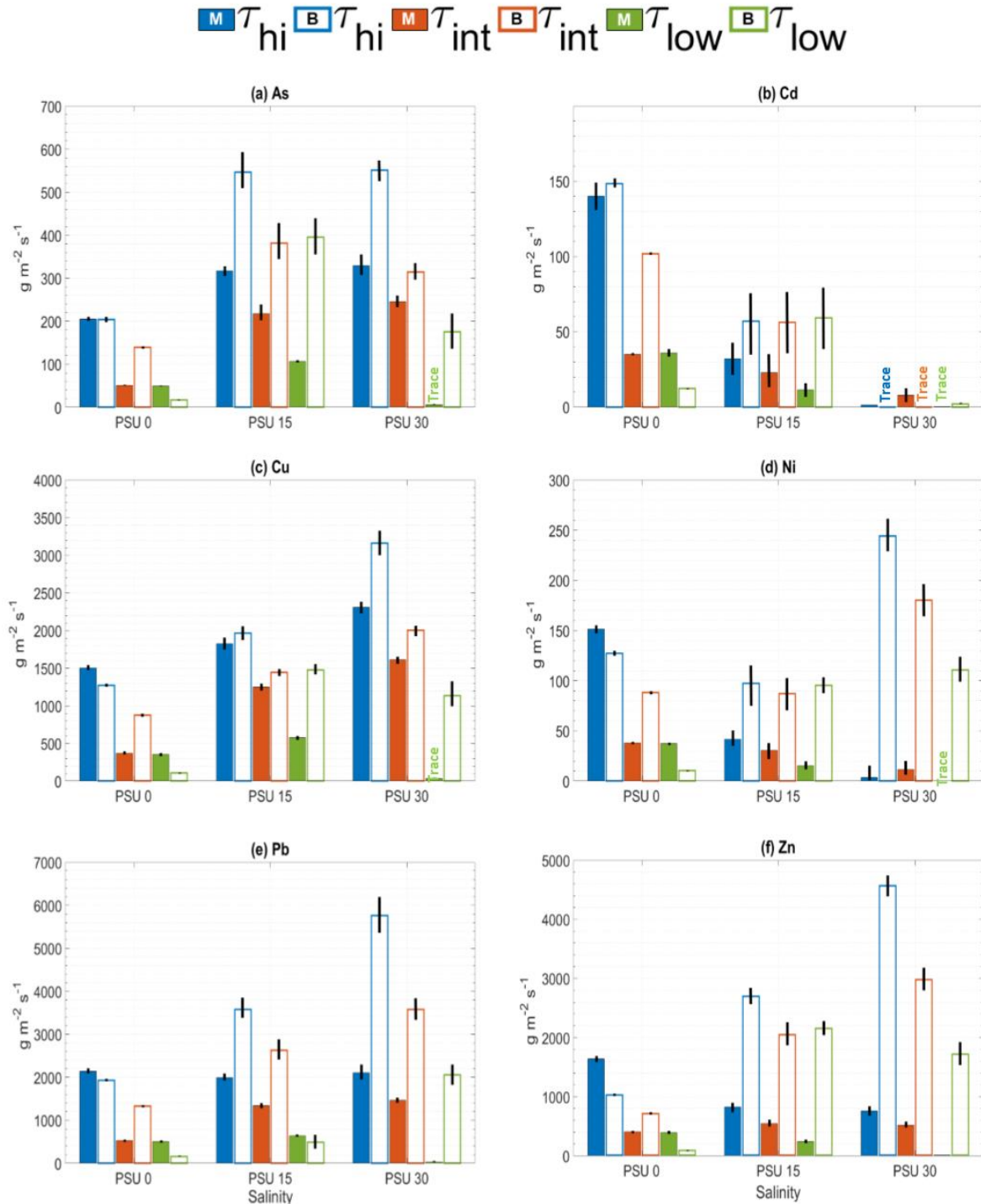
$$464 \quad PSF = C_d \times MSF \quad [Eq. 3]$$

465 where MSF = mass settling flux ($\text{g m}^{-1}\text{s}^{-1}$) and C_d = mass of PTM on particulates (mg kg^{-1}).

466 Particulate settling fluxes (PSF) for each PTM in each experimental run are shown in Figure 4
467 and Table S5. A comparison across each turbulent shear stress reveals that deposition rates for
468 all PTMs are greatest (for biotic and mineral) under the highest turbulence (τ_{Hi}) conditions.

469 *PSF*, however, varies between PTMs with salinity. For As *PSF* increases moving from 0 to 15
470 PSU then then is similar or even decreases from 15 to 30 PSU, with $PSF_{(bio)}$ being significantly
471 greater than the mineral equivalent. For Cd, there was a reduction in both *PSF* for both biotic
472 and mineral with increases in salinity, again with rates greatest under biotic conditions. Copper
473 showed a generally increasing trend with salinity, although at low shear strength the *PSF* did
474 decrease for both $PSF_{(bio)}$ and $PSF_{(min)}$. For Ni and Zn comparison between the biotic and
475 mineral tests were not consistent. *PSF* decreased consistently with salinity for the mineral
476 experiments (particularly for Ni) but for the biotic conditions with EPS added, rates were
477 highest for the 30 PSU conditions and were generally higher for the biotic tests compared with
478 equivalent mineral ones. At 30 PSU the *PSF* showed a significant downward trend from high
479 to low shear stress, which was not obvious for the mineral equivalent tests, although this may
480 have been a result of *PSF* values being very low for Ni and Zn in these experiments making
481 trends hard to discern. Lead exhibited increasing *PSF* with salinity for the biotic tests, with a
482 trend of the *PSF* being highest for high turbulence and lowest for lowest shear stresses. For the
483 mineral tests under high turbulence, Pb *PSF* changed little with salinity, but at intermediate
484 and low turbulence *PSF* tended to increase between 0 and 15 PSU then decrease slightly at the
485 highest PSU, with the rates at the intermediate turbulence being commensurately higher than
486 the low shear stress conditions.

487 Table S6 shows *PSF* values for each PTM ranked by magnitude for SPM type, salinity and
488 turbulent shear stress. Across all experimental runs and for biotic SPM the order of magnitude
489 of *PSF* is Pb>Zn>Cu>As>Ni>Cd. For mineral SPM, the same order holds except that Cu>Zn.
490 Comparison of highest and lowest values shows Pb is deposited at 45, 38 and 49 times the rate
491 of Cd for all, mineral and biotic SPM, respectively.



492

493 **Figure 4: Settling flux of particulate PTM, PSF , for each PTM for each experimental**

494 **run. Solid bars indicate results for mineral SPM; bars with colour outlines**

495 **indicate results for biotic SPM. Error bars are confidence intervals at 95%.**

496

497 Table S6b shows that particulate Pb is consistently deposited at the highest rate for each
498 salinity. Cadmium exhibits the lowest rate of deposition for saline conditions, Ni for
499 freshwater. Comparison of highest and lowest values shows that Pb is deposited 14 times faster
500 than Ni in freshwater, 45 times faster than Cd in estuarine salinity and 1,362 times faster for
501 ocean salinity.

502 **4. CONCLUSION**

503 Estuaries act as a critical conduit for the transfer of terrestrially-derived metal pollutants to
504 coastal waters. By simulating the typical range of shear stresses, salinities and EPS contents
505 within a cohesive estuarine environment this study has generated a dataset with which
506 modellers and estuarine chemists can begin to untangle the complex interactions between the
507 bio-physico-chemical processes controlling the fate of PTMs.

508 The data presented in this study has highlighted that the dynamic nature of an estuarine
509 environment that leads to a constantly varying sorption dynamic between the main bio-physico-
510 chemical parameters. This study reveals that salinity has the most significant role in dictating
511 the particulate-phase settling flux of a range of common metal pollutants; the presence of EPS
512 has a moderate effect; and changes to turbulent shear stress cause the least variation.

513 While the effects of chloro-complexation are well-known, the role of EPS is less understood.
514 Other studies have reported the importance of dissolved organic matter in controlling the
515 partitioning of metals in contaminated estuaries via organic colloidal matter stabilising metals
516 in the dissolved phase (Wang et al., 2017). As has been shown in this study, there is a
517 complex interplay between the PTMs, complexation by dissolved organic matter and the role
518 organic compounds, particularly EPS, play in both complexation but also the particle
519 flocculation process. The results show that the presence of EPS considerably modifies
520 sorption dynamics. Under freshwater conditions it reduces K_p for all PTMs compared with

521 mineral-only conditions. Conversely, in most cases under saline conditions K_p is greater when
522 EPS is present.

523 Results highlight the importance of considering cohesive sediments in understanding the fate
524 of PTMs. Flocs are porous and therefore offer a greater area for PTM sorption. Changes in
525 floc size and suspended particulate matter concentrations also influence the sorption
526 characteristics of the flocculating particles. Flocculation efficiency is enhanced by the
527 presence of EPS in freshwater (see also Zhou et al., 2011), generating larger, more porous
528 flocs with lower densities. While salinity acts to reduce the influence of EPS in binding
529 particles compared to freshwater, total surface area is larger than biotic conditions due to
530 greater floc frequency and lower settling rates, which maintains flocs in suspension.

531 Consequently, EPS increases the rate at which sediment settles under saline conditions, driven
532 by a lower settling velocity and higher effective density compared with mineral-only flocs.

533 Parameters such as effective floc density and settling velocities have been shown in this study
534 to span several orders of magnitude which has commensurate impacts on the partitioning of
535 the PTMs between the dissolved and particulate phases. Moreover, an accurate representation
536 of particulate-phase metal settling flux in cohesive sediments can only be achieved by
537 characterizing the temporal and spatial variations in the mass settling flux of the flocculated
538 suspended sediment. The deposition rates calculated here reflect the partition coefficients of
539 the individual PTMs, which has been well reported for the natural estuarine environment
540 (Comber et al., 1995; Turner et al., 2002), however the value of combining the partitioning
541 characteristics of the PTMs with the sediment flocculation dynamics allows the estimation of
542 flux of metals accumulating within sediments over time. The combination of changing
543 partitioning coefficients and settling flux of the sediment yields several orders of magnitude
544 difference in the deposition rate of metals bound to the sediment. The settling rate of particle-
545 bound metals tends to be greatest for biotic rather than mineral-only sediments in saline

546 water. The pattern is reversed in freshwater largely due to lower K_p values resulting from the
547 presence of EPS.

548 Incorporation of the metals into organic-rich particulate matter may also act as a way of
549 stabilising the metal in the sedimentary phase, contributing to the diagenesis of the PTMs and
550 removal from any further biological processing (Jokinen et al., 2020). With a knowledge of
551 turbulence associated with an estuarine environment, with these deposition rate calculations it
552 would be possible to determine areas of sediment and therefore metal accumulation and
553 therefore identify parts of estuaries most likely to be at risk of levels building up to be a risk to
554 benthic flora and fauna or are being sequestered, thus decreasing their risk.

555 There is a growing interest and concern regarding the influence sediment bound PTMs on in
556 situ organisms and its interaction with overlying waters (Environment Agency, 2018). The data
557 presented in this study highlights the need to consider a holistic approach to determining the
558 fate of PTMs, from above the tidal limit to the coastal zone, taking account of the highly
559 dynamic spatial and temporal nature of these environments. Although flocculation is secondary
560 to salinity in terms of partitioning, it plays a critical role in sediment deposition and therefore
561 PTM accumulation in bed sediments, with EPS significantly impacting on the partitioning and
562 flocculation processes. Undertaking any risk assessment or modelling not taking account of the
563 impacts of EPS on the partitioning of PTMs within a dynamic sediment environment are likely
564 to lead to a bias in any outcomes or predictions.

565 Measurement of metals and flocculated sediments is resource intensive and logistically
566 difficult, not least in developing countries or remote locations. Consequently, numerical
567 modelling plays an important role in understanding the fate of dispersed metals. This study
568 offers a framework in which to develop improved numerical modelling parameterisations of
569 both soluble and particulate-phase PTMs. The provision of partitioning coefficients that
570 represent the response of each metal to biological, physical and chemical variations provide a

571 basis for a dynamic partitioning coefficient. When implemented within combined flow &
572 sediment models, particularly those that consider flocculation, relative proportions of soluble
573 and particulate-phase metal content can be subject to appropriate flow and sediment transport
574 calculations. Such an approach facilitates the management of environmental threats in the
575 short-term, e.g., an at-a-point accidental release of PTMs, or in the long-term, e.g., the
576 accumulation of PTMs in different spatial locations within a catchment.

577 **Acknowledgements:**

578 The authors would like to thank Dr's Andy Fisher and Rob Clough for assistance in the
579 analytical aspects of this work. The work was funded by Plymouth University's Seale Hayne
580 Educational Trust and Marine Institute.

581 **Conflict of Interest Statement**

582 The authors can confirm that there are no conflicts of interest associated with this work.

583 **References**

- 584 Benoit G., Oktay-Marshall S.D., Cantu II A., Hood E.M., Coleman C.H., Corapcioglu M.O.,
585 Santschi P.H., Partitioning of Cu, Pb, Ag, Zn, Fe, Al, and Mn between filter retained particles,
586 colloids, and solution in six Texas estuaries, *Marine Chemistry*, 45, pp 307-336, 1994.
- 587 Gerbersdorf, S. U., Westrich, B., Paterson, D. M. Microbial extracellular polymeric substances
588 (EPS) in fresh water sediments. *Microb. Ecol.* 58, 334–349, 2009.
- 589 Black, K. S., T. J. Tolhurst, T.J., Paterson, D. M., Hagerthey, S. E., Working with natural
590 cohesive sediments, *Journal of Hydraulic Engineering*, 128, 2–8, 2002.
- 591 Comber, S.D.W., Gardner M.J., Gunn A.M., Whalley C., Kinetics of trace metal sorption to
592 estuarine suspended particulate matter. *Chemosphere*, 33, 1027-1040, 1996.

593 Comber, S.D.W., Gunn A.M., Whalley, C., Comparison of the partitioning of trace metals in
594 the Humber and Mersey estuaries. *Marine Pollution Bulletin*, 30, 851-860, 1995.

595 Defonseca E.M., Neto J.A., McAlister J., Smith B., Fernandez M.A. and Baliero F.C. The role
596 of the humic substances in the fractioning of heavy metals in Rodrigo de Freitas Lagoon, Rio
597 De Janeiro, Brazil. *Annals of the Brazilian Academy of Sciences*, 85, 1289-1301, 2013.

598 DEFRA, Water Framework Directive implementation in England and Wales: new and updated
599 standards to protect the water environment, UK, 44 pp, 2014.

600 Dennis, I.A., Macklin, M.G., Coulthard, T.J., Brewer, P.A., The impact of the October–
601 November 2000 floods on contaminant metal dispersal in the River Swale catchment, North
602 Yorkshire, UK, *Hydrological Processes*, 17, 1641-1657, 2003.

603 Dyer, K., Manning, A.J., Observation of the size, settling velocity and effective density of flocs,
604 and their fractal dimensions. *Journal of Sea Research*, 41, pp 87-95, 1998.

605 Elliott, M. and McLusky, D.S., The need for definitions in understanding estuaries. *Estuarine,
606 Coastal and Shelf Science*, 55, 815-827, 2002.

607 Environment Agency, Water Framework Directive, Update, 131 pp, 2011.

608 Environment Agency. SeDiChem Technical Report, Impact of sediment disturbance on
609 chemical status. Report no. EcoSF2/18/269, 2018.

610 Feng C., Guo X., Tian C. and Li Y. Heavy metal partitioning of suspended sediment matter-
611 water and sediment-water in the Yangtze estuary. *Chemosphere*, 185, 717-725, 2017.

612 Hanlon A.R.M., Bellinger B., Haynes K., Xiao G., Hofmann T.A., Gretz M.R., Ball A.S.,
613 Osborn A.M., Underwood G.J.C. Dynamics of extracellular polymeric substance (EPS)
614 production and loss in an estuarine, diatom-dominated, microalgal biofilm over a tidal
615 emersion–immersion period. *Limnol. Oceanogr.*, 1, 79-93, 2006.

616 Healy, T., Wang, Y., Healy, J.A., Muddy Coasts of the World: Processes, Deposits and
617 Function: Amsterdam, Elsevier, 556 pp, 2002.

618 Heiro A., Olias M., Canovas C.R., Martin J.E. and Bolivar J.P. Trace metal partitioning over a
619 tidal cycle in an estuary affected by acid mine drainage (Tinto estuary, SW Spain). *Sci. of the*
620 *Tot. Environ.*, 497-498, 18-28, 2014.

621 Hong S., Candelone J.P., Patterson C.C., Boutron C.F., History of ancient copper smelting
622 pollution during roman and medieval times recorded in green land ice, *Science*, 1669;
623 272(5259), pp 246–249, 2018.

624 Howarth R. W., J. R. Fruci J.R., Sherman D., Input of sediment and carbon to an estuarine
625 ecosystem: Influence of land use. *Ecological Applications*, 1, pp 27–39, 1991.

626 Hudson-Edwards, K.A., Macklin, M.G., Taylor, M.P. 2000 years of sediment-borne heavy
627 metal storage in the Yorkshire Ouse basin, NE England, UK, *Hydrological Processes*, 13,
628 1087-1102, 1999.

629 Jokinen S.A., Jilbert T., Filppula R.T. and Koho K., Terrestrial organic matter input drives
630 sedimentary trace metal sequestration in a human impacted boreal estuary. *Sci. of the Tot.*
631 *Environ.*, 717, 137047, 2020.

632 Kiørboe, T., Formation and fate of marine snow: small-scale processes with large- scale
633 implications, *Scientia Marina*, 65, 57-71, 2001.

634 Klimpel R.C., Hogg R., Effects of flocculation conditions on agglomerate structure. *Journal of*
635 *Colloid Interface Science*, 113, pp 121-131, 1986.

636 Koron, N., Faganeli, J., Falnoga, I., Mazej, D., Klun, K., Kovac, N., Association of
637 macroaggregates and metals in coastal waters, *Marine Chemistry*, 157, pp 185-193, 2013.

638 Lai H., Fang, H., Huang, L., He, G., Reible, D. A review on sediment bioflocculation:
639 Dynamics, influencing factors and modelling, *Science of the Total Environment*, 642, 1184-
640 1200, 2018.

641 Luoma S.N., Rainbow P.S., Metal contamination in aquatic environments. Science and lateral
642 management, New York, U.S.A., 573 pp, 2008.

643 Machado, A.A.S., Spencer, K., Kloas, W., Toffolon, C.Z., Metal fate and effects in estuaries:
644 A review and conceptual model for better understanding of toxicity, *Science of the Total*
645 *Environment*, 541, 268-281, 2016.

646 Malarkey, J., Baas, J.H., Hope, J.A., Aspden, R.J., Parsons, D.R., Peakall, J., Paterson, D.M.,
647 Schindler, R.J., Ye, L., Lichtman, I.D., Bass, S.J., Davies, A.G., Manning, A.J., & Thorne,
648 P.D. The pervasive role of biological cohesion in bedform development, *Nature*
649 *Communications*, 6, 6257-6261, 2015.

650 Manning A.J., Dyer K.R., A laboratory examination of floc characteristics with regard to
651 turbulent shearing, *Marine Geology*, 160, 147-170, 1999.

652 Manning A.J., Whitehouse R.J.S., Plymouth University Mini-annular flume – operation and
653 hydrodynamic calibration. HR Wallingford Technical Report TR 169, UK, 2009.

654 Manning A.J., Observations of the properties of flocculated cohesive sediment in three Western
655 European estuaries. *Journal of Coastal Research Special Issue*, SI 41, pp 70–81, 2004.

656 Manning, A.J., Whitehouse, R.J.S., Uncles, R.J. Suspended particulate matter: the
657 measurements of flocs. In: R.J. Uncles and S. Mitchell (Eds), *ECSA practical handbooks on*
658 *survey and analysis methods: Estuarine and coastal hydrography and sedimentology*, pp. 211-
659 260, Pub. Cambridge University Press, 2017.

660 Matta J., Milad M., Manger R., Tosteson T., Heavy metals, lipid peroxidation, and
661 cigateratoxicity in the liver of the Caribben barracuda (*Sphyaena barracuda*), *Biological Trace*
662 *Element Research*, 70 , pp. 69-79, 1999.

663 Meadows, P.S., Meadows, A., Murray, J.M.H., *Biological modifiers of marine benthic*
664 *seascapes: Their role as ecosystem engineers*, *Geomorphology*, 157–158, 31–48, 2012.

665 *Millennium Ecosystem Assessment: Ecosystems and Human Well-Being*, (Eds.) Sarukhan, J.,
666 Whyte, A., Hassan, R., Scholes, R., *Island Press*, Washington, DC, 2005.

667 Miller J.R, Lechler P.J, Mackin G., Germanoski D., Villarroel L.F., *Evaluation of particle*
668 *dispersal from mining and milling operations using lead isotopic fingerprinting techniques*, *Rio*
669 *Pilcomayo Basin, Bolivia*, *Science of The Total Environment*, 384, pp 355-373, 2007.

670 McCave I.N., *Size spectra and aggregation of suspended particles in the deep ocean*, *Deep-Sea*
671 *Research*, 31, pp 329-352, 1984.

672 Morelle J., Schapira M. and Claquin P. *Dynamics of phytoplankton productivity and*
673 *exopolysaccharides (EPS and TEP) pools in the Seine Estuary (France, Normandy) over*
674 *tidal cycles and over two contrasting seasons*. *Mar. Environ. Res.*, 131, 162-176, 2017.

675 Motekaitis R.J. and Martell A.E., *Speciation of metals in the oceans. i. Inorganic complexes in*
676 *seawater, and influence of added chelating agents*. *Marine Chemistry*, 21, 101-116, 1987.

677 Nho N.T., Strady E., Trang T., David F. and Marchand C. *Trace metals partitioning between*
678 *particulate and dissolved phases along a tropical mangrove estuary (Can Gio, Vietnam)*.
679 *Chemosphere*, 196, 311-322, 2018.

680 Parsons, D. .R., Schindler, R.J., Hope, J.A., Malarkey, J., Baas, J.H., Peakall, J., Manning,
681 A.J., Ye, L., Simmons, S., Paterson, D.M., Aspden, R.J., Bass, S.J., Davies, A.G., Lichtman,
682 I.D., Thorne, P.D., *The role of bio-physical cohesion on subaqueous bedform size*, *Geophysical*
683 *Research Letters*, 43, 1566–1573, 2016.

684 Paterson, D.M., Yallop, M.L., Wellsbury, P., Inter-relationships between rates of microbial
685 production, exopolymer production, microbial biomass and sediment stability in biofilms of
686 intertidal sediments, *Microbial Ecology*, 39, 116-127, 2000.

687 Singh K.P., Malik A., Sinha S., Estimation of Source of Heavy Metal Contamination in
688 Sediments of Gomti River (India) using Principal Component Analysis. *Water Air & Soil
689 Pollution*, 166, 321–341, 2005.

690 SKB, Solid/liquid partition coefficients (K_d) for selected soils and sediments at Forsmark and
691 Laxemar-Simpevarp, Denmark, 102 pp, 2009.

692 Spears B.M., Saunders J.E., Davidson I., Paterson D.M. Microalgal sediment biostabilisation
693 along a salinity gradient in the Eden Estuary, Scotland: unravelling a paradox. *Marine and
694 freshwater Research*, 59, 313-321, 2007.

695 Spencer, K.L., MacLeod, C.L., Tuckett, A., Johnson, S.M., Source and distribution of trace
696 metals in the Medway and Swale estuaries, Kent, UK, *Marine pollution Bulletin*, 52, 214-238,
697 2006.

698 Taylor M.P., Hudson-Edwards, K.A., The dispersal and storage of sediment-associated metals
699 in an arid river system: The Leichhardt River, Mount Isa, Queensland, Australia,
700 *Environmental Pollution*, 152, 193-204, 2008.

701 Turner A., Millward G.E., Suspended Particles: Their Role in Estuarine Biogeochemical
702 Cycles, *Estuarine, Coastal and Shelf Science*, 55, 857-883, 2002.

703 Turner, A., Trace-metal partitioning in estuaries: importance of salinity and particle
704 concentration. *Marine Chemistry*, 54, 27-39, 1996.

705 Turner A. Millward G.E., LeRoux S.M. Significance of oxides and particulate organic matter
706 in controlling trace metal partitioning in a contaminated estuary. *Mar. Chem.*, 88, 179-192,
707 2004.

708 Van der Auweraert E. (2018) Trace metal pollution in the Scheldt estuary – a statistical
709 approach to estimate metal partitioning coefficient for a suite of metals. PhD Thesis, Delft
710 University of Technology, Sept 30, 2018.

711 Wang W. and Wang W.X. Phase partitioning of trace metals in a contaminated estuary
712 influenced by industrial effluent discharge. *Environmental Pollution*, 214, 35-44, 2016.

713 Wang W., Chen M., Guo L. and Wang W.X. Size partitioning and mixing behaviour of trace
714 metals and dissolved organic matter in a south China Estuary. *Sci. of the Tot. Environ.*, 603-
715 604, 434-444, 2017.

716 Wells R., Impact of sediment disturbance on chemical status. Environment Agency report
717 SC180002, UK, 53 pp, 2019.

718 Zwolsman, J.J.G, Berger, G.W., Van Eck, G.T.M., Sediment accumulation rates, historical
719 input, post-depositional mobility and retention of major elements and trace metals in salt marsh
720 sediments of the Scheldt estuary, SW Netherlands, *Marine Chemistry*, 44, 73-94, 1993.